



UvA-DARE (Digital Academic Repository)

Optimization of adaptive radiation therapy in cervical cancer: Solutions for photon and proton therapy

van de Schoot, A.J.A.J.

Publication date

2016

Document Version

Final published version

[Link to publication](#)

Citation for published version (APA):

van de Schoot, A. J. A. J. (2016). *Optimization of adaptive radiation therapy in cervical cancer: Solutions for photon and proton therapy*. [Thesis, fully internal, Universiteit van Amsterdam].

General rights

It is not permitted to download or to forward/distribute the text or part of it without the consent of the author(s) and/or copyright holder(s), other than for strictly personal, individual use, unless the work is under an open content license (like Creative Commons).

Disclaimer/Complaints regulations

If you believe that digital publication of certain material infringes any of your rights or (privacy) interests, please let the Library know, stating your reasons. In case of a legitimate complaint, the Library will make the material inaccessible and/or remove it from the website. Please Ask the Library: <https://uba.uva.nl/en/contact>, or a letter to: Library of the University of Amsterdam, Secretariat, P.O. Box 19185, 1000 GD Amsterdam, The Netherlands. You will be contacted as soon as possible.

Chapter 3

Generic method for automatic bladder segmentation on cone beam CT using a patient-specific bladder shape model

A version of this chapter has been published as:

Generic method for automatic bladder segmentation on cone beam CT using a patient-specific bladder shape model

A.J.A.J. van de Schoot, G. Schooneveldt, S. Wognum, M.S. Hoogeman, X. Chai, L.J.A. Stalpers, C.R.N. Rasch and A. Bel

Medical Physics 2014; 41(3): 031707.

<http://dx.doi.org/10.1118/1.4865762>

Abstract

Purpose

The aim of this study is to develop and validate a generic method for automatic bladder segmentation on CBCT, independent of gender and treatment position (prone or supine), using only pre-treatment imaging data.

Material & Methods

Data of twenty patients, treated for tumors in the pelvic region with the entire bladder visible on CT and CBCT, were divided into four equally sized groups based on gender and treatment position. The full and empty bladder contour, that can be acquired with pre-treatment CT imaging, were used to generate a patient-specific bladder shape model. This model was used to guide the segmentation process on CBCT. To obtain the bladder segmentation, the reference bladder contour was deformed iteratively by maximizing the cross-correlation between directional grey value gradients over the reference and CBCT bladder edge. To overcome incorrect segmentations caused by CBCT image artifacts, automatic adaptations were implemented. Moreover, locally incorrect segmentations could be adapted manually. After each adapted segmentation, the bladder shape model was expanded and new shape patterns were calculated for following segmentations. All available CBCTs were used to validate the segmentation algorithm. The bladder segmentations were validated by comparison with the manual delineations and the segmentation performance was quantified using the Dice similarity coefficient (DSC), surface distance error (SDE) and SD of contour-to-contour distances. Also, bladder volumes obtained by manual delineations and segmentations were compared using a Bland-Altman error analysis.

Results

The mean DSC, mean SDE and mean SD of contour-to-contour distances between segmentations and manual delineations were 0.87, 0.27 cm and 0.22 cm (female, prone), 0.85, 0.28 cm and 0.22 cm (female, supine), 0.89, 0.21 cm and 0.17 cm (male, supine) and 0.88, 0.23 cm and 0.17 cm (male, prone), respectively. Manual local adaptations improved the segmentation results significantly ($p < 0.01$) based on DSC (6.72%) and SD of contour-to-contour distances (0.08 cm) and decreased the 95% confidence intervals of the bladder volume differences. Moreover, expanding the shape model improved the segmentation results significantly ($p < 0.01$) based on DSC and SD of contour-to-contour distances.

Conclusion

This patient-specific shape model based automatic bladder segmentation method on CBCT is accurate and generic. Our segmentation method only needs two pre-treatment imaging data sets as prior knowledge, is independent of patient gender and patient treatment position and has the possibility to manually adapt the segmentation locally.

3.1 | Introduction

Image-guided radiation therapy (IGRT) using daily cone beam computed tomography (CBCT) aims to safeguard the delivery of the planned dose to the patient [86,87]. However, anatomical deformations in patients limit the benefits of IGRT, since a straightforward positional correction is often not possible. The pelvic region contains several organs, e.g. bladder, rectum and cervix-uterus or prostate, with large daily variation in size and position during fractionated radiation therapy (RT) [64,88–91]. To compensate for these geometrical uncertainties, large safety margins around the target volume have to be applied [92,93]. However, these margins result in a high dose to surrounding healthy tissue and are in some cases even insufficient [94,95].

Adaptive radiation therapy (ART) is increasingly used to correct for these large interfraction deformations during fractionated RT and can be applied using several strategies, dependent on the size of deformations and position verification possibilities [53,96–98]. Originally, ART was developed as an offline strategy to correct for systematic errors by re-planning during the course of RT [47,48]. However, this adaptive strategy induces additional clinical workload during RT [56]. More recently, an alternative practical approach of ART using a multiple-plan strategy has been applied more frequently [60,63,83,98,99]. Several treatment plans are designed in advance based on pre-treatment imaging with substantial target variation in size and position. Each treatment day the plan corresponding best with the target position, the plan-of-the-day, will be selected while the patient is positioned correctly on the treatment table. This online plan selection procedure is based on daily CBCT imaging and will lead to less irradiated healthy tissue without reducing CTV coverage [60,99]. Consequently, this can lead to the use of smaller CTV-to-PTV margins in future. In this plan-of-the-day approach for tumors in the pelvic region the bladder plays a crucial role, either as a deforming target organ in the case of bladder tumors [60,98,99] or as an organ at risk (OAR) influencing the target position for cervix-uterus tumors [64,83] or prostate tumors [97]. Therefore, daily quantification of the size and position of the bladder will be of interest in those adaptive strategies.

Automatic organ segmentation on daily CBCT images is challenging due to the poor soft tissue contrast and the various reconstruction artifacts [100], but it is required for online recalculation of the dose [101] or adequate image guidance [102,103]. Furthermore, automatic segmentation of the bladder on daily CBCT images will facilitate multiple-plan ART in different ways. To accumulate the delivered dose to the bladder correctly, the daily size and position of the bladder need to be determined [104,105]. Moreover, automatic bladder segmentation can facilitate plan-of-the-day selection from a library of plans by decreasing the observer dependency and decision time in the treatment room [63,106,107].

Previously, two automatic bladder segmentation methods on CBCT were developed in our group [106,107]. However, both methods have limitations in their application for multiple-plan ART. The first proposed segmentation method was based on a training set acquired with the first five CBCTs and is hampering the application from the start of the adaptive treatment

[106]. The second proposed method used a population-based bladder shape model to guide the segmentation [107]. However, this population-based model needed a sufficient number of bladder shapes to describe all patient-specific shape variations and for each gender and treatment position a population-based bladder shape model would have to be created. Also, both proposed methods have only been applied and tested on male patients treated in supine position.

In this study, we added a number of improvements to the earlier automatic bladder segmentation methods on CBCT and validated this method for different patient groups. To enable the segmentation for the various patient groups, independent of gender and position on the treatment table (prone or supine), only patient-specific bladder shape information based on pre-treatment imaging data was used. For each patient, a model was built to estimate the patient-specific bladder shape variation from the start of treatment and this model was expanded during treatment. The aim of this study is to present a generic method for automatic bladder segmentation on CBCT for each gender and treatment position using only patient-specific pre-treatment imaging data.

3.2 | Material & Methods

Patient data

Imaging data (CT and CBCT) of 20 patients were selected, who were treated for tumors in the pelvic region with the entire bladder visible on CT and CBCT. The CT images (LightSpeed RT16 system, General Electric Company, Waukesha WI, USA) were acquired with a pixel size of $1.0 \times 1.0 \text{ mm}^2$ and a slice thickness of 2.5 mm. The resolution of the CBCT images (Synergy, Elekta Oncology systems, Crawley, UK) were either $410 \times 410 \times 264$ or $410 \times 410 \times 120$, with a pixel size of $1.0 \times 1.0 \text{ mm}^2$ and a slice thickness of 1.0 mm. The acquisition parameters of the CBCT projection images were either 120 kV, 40 mA, 40 ms per projection or 120 kV, 32 mA, 40 ms per projection.

Since the bladder position, bladder shape and the bladder deformation vary between both the gender of the patient and its treatment position [26,91,106], the data of these patients were divided into four equally sized subgroups based on gender and treatment position (Table 3.1). Each patient had a median of 7 (range, 5–9) CBCT images, all acquired for position verification purposes. As part of the clinical routine for treatment planning purposes, the outer boundary of the bladder on CT images were manually delineated slice-by-slice by a radiation oncologist. The outer boundary of the bladder on all CBCT images were manually delineated slice-by-slice by one observer and revised by an experienced radiation therapy technologist (RTT).

Since we used retrospective patient data, only one pre-treatment CT was available for each included patient. According to the clinical protocol, this CT was acquired with a full bladder. Due to the absence of an empty bladder CT for these patients, the CBCT image with the emptiest bladder was used as a surrogate. All other CBCT images were used to validate the segmentation algorithm.

Table 3.1 | Characteristics of the different patient groups, with five patients in each group. All patients were treated with IMRT. Patients treated in prone position were lying on a belly board [26].

Group	Gender	Treatment position	Treatment site	Fractionation scheme (Gy)	Total CBCTs	Bladder volume range (ml)				
						Patient 1	Patient 2	Patient 3	Patient 4	Patient 5
A	Female	Prone	Cervix-Uterus	23 x 2.00	36	122–487	77–381	90–502	165–359	86–506
B	Female	Supine	Cervix-Uterus	23 x 2.00	29	60–200	98–311	141–403	187–356	48–114
C	Male	Supine	Bladder (1–4) Prostate (5)	20 x 2.75 35 x 2.20	37	145–189	158–216	53–375	82–106	91–406
D	Male	Prone	Rectum	28 x 1.80	37	78–335	114–199	100–446	173–259	94–332

Abbreviations: CBCT = cone-beam computed tomography; Gy = gray.

Bladder segmentation

This novel method of automatic bladder segmentation on CBCT images consisted of three main parts. First, for each patient a principal component analysis (PCA) based statistical model was built to estimate the patient-specific bladder shape variation from the full bladder contour and the empty bladder contour. Second, this patient-specific bladder shape model was used in an online 3D segmentation process to segment the bladder on CBCT images. Finally, the resulting segmentation can be improved locally by manual adaptations and this adapted bladder segmentation was included in the model for ensuing segmentations.

Patient-specific bladder shape model

For each patient, a unique patient-specific bladder shape model was built prior to treatment using only the manually delineated full and empty reference bladder contours. To create this shape model, both contours were aligned by registering the image with the full bladder to the image with the empty bladder based on bony anatomy. Next, the contours were transformed to 3D triangular surface meshes. To eliminate unnatural shape differences, both 3D triangular surfaces were smoothed using a non-shrinkage smoothing method [108].

The smoothed bladder surfaces were described with an equal number of points and triangular connections. To do so, a uniform 3D sphere surface was created with an arbitrary chosen and evenly distributed number of vertices ($M=2091$). The central point of this sphere (O_{sphere}) was automatically positioned at the center of the empty bladder contour and consequently inside both bladder surfaces. The smoothed bladder surfaces were resampled in 3D at the intersection of the spherical radial lines passing through the central point and bladder surface. These 2091 lines in radial direction were assumed to be dense enough to fully capture the feature points of bladder surfaces.

The resampled bladder surface shape vectors in Cartesian coordinates were represented in spherical coordinates using O_{sphere} as origin. Next, we applied a spherical harmonic transformation to both bladder surfaces, as described by Chai *et al.* [107] and Brechbühler *et al.* [109]. The bladder

surfaces were described using vectors consisting of spherical harmonic coefficients up to degree K , representing spatial variation of the bladder surface. Spatial variation was defined as the mean distance between corresponding points on the original bladder surface and the bladder surface described using K degrees. In this study, the degree $K=7$ was used as upper limit to model spatial variation of bladder surfaces, as that was sufficient to achieve a mean distance error smaller than 0.10 cm for all bladder surfaces.

After resampling and spherical harmonic transformation, the full and empty bladder surface were described by a unique shape parameter vector (ω_i) consisting of $3(K+1)^2=192$ spherical harmonic coefficients [107]. It was assumed that the set of shape parameter vectors could be seen as samples from a random process. For anatomical reasons, displacements of vertices and bladder deformation are highly correlated. This implies that the underlying dimensionality of this multivariate statistical problem is much smaller than the number of vertices and thus the correlated displacements of the surface points can be described using PCA [110]. This method reduces the dimensionality of the shape parameter vector by computing the major modes of shape variation.

First, the mean shape parameter vector ($\bar{\omega}$) was calculated from the shape parameter vectors (ω_i) (Equation 3.1) and the mean shape vector was used to determine the covariance matrix (C) (Equation 3.2). Next, the eigenvector (v) and associated eigenvalue (λ) were determined by eigendecomposition of the covariance matrix (Equation 3.3). The determined eigenvectors of this covariance matrix represented the bladder deformation pattern based on the full and empty bladder contours.

$$\bar{\omega} = \frac{1}{N} \sum_{i=1}^N \omega_i \quad (3.1)$$

$$C = \frac{1}{N-1} \sum_{i=1}^N (\omega_i - \bar{\omega}) \cdot (\omega_i - \bar{\omega})^T \quad (3.2)$$

$$C\lambda = \lambda \lambda \quad (3.3)$$

Segmentation process

The input of the segmentation algorithm was the CBCT image to be segmented, a reference image with delineated bladder contour and the patient-specific bladder shape model. In order to suppress noise, the grey values of both the reference image and the CBCT image were smoothed by an isotropic 3D Gaussian smoothing filter with a standard deviation (SD) of 0.3 cm. This value was optimized in a previous study and based on a different patient population [106]. Next, the images were registered based on bony anatomy by using the clinically obtained translation vector after CT image and CBCT image alignment.

The process of segmentation was similar to the segmentation process described in detail by Chai *et al.* [107]. The process started with a delineated bladder contour from pre-treatment imaging as initial segmentation and this contour was deformed iteratively according to the deformation patterns calculated from the patient-specific bladder shape model. The segmentation

was obtained by minimizing a cost function (CF) (Equation 3.4), based on the cross-correlation between directional internal and external grey value gradients over the reference bladder contour (G_R) and the segmented bladder contour (G_S) (Equation 3.5). To find the bladder shape that best corresponds with the reference bladder contour within the interval $[-3, 3]$, a simplex optimizer was used for cost function minimization [111]. The process of optimization was completed when the cost function value difference between two consecutive iterations was below $5.0e^{-5}$.

$$CF=2-(CC(G_R^{int}, G_S^{int}) + CC(G_R^{ext}, G_S^{ext})) \quad (3.4)$$

$$CC(G_R, G_S) = \frac{\sum_{i=1}^M (G_R(i) - \bar{G}_R)(G_S(i) - \bar{G}_S)}{\sqrt{\sum_{i=1}^M (G_R(i) - \bar{G}_R)^2} \sqrt{\sum_{i=1}^M (G_S(i) - \bar{G}_S)^2}} \quad (3.5)$$

Automatic adaptations

As observed by Chai *et al.* [107], the algorithm could produce an incorrect bladder segmentation after regular cost function minimization due to various causes. Image artifacts on CBCT could produce fictitious bladder edges, the cost function optimization could end in a local minimum or large anatomical differences between reference structure and the structure on CBCT could cause different grey value gradient fields. To avoid segmentation failure caused by these artifacts, several automatic fine-tuning mechanisms were implemented that were not present in the approach by Chai *et al.* [107].

The first automatic fine-tuning mechanism is the implementation of different starting points and different reference contours. The contours of the full and empty bladder were both used as initial contour at the start of the segmentation. In addition, both contours were used as reference contours, combined with their associated imaging data. Consequently, the process of segmentation was done four times: two different initial contours and two different reference contours. The segmentation with the lowest cost function result was considered the best segmentation and therefore selected as final bladder segmentation.

Another fine-tuning mechanism was introduced to overcome incorrect segmentations caused by dominating inconsistent grey value gradients. For example, if a part of the bladder edge in the reference image was located next to bony structure, the directional grey value gradients became large and dominated the cost function. To decrease the influence of vertices with large gradient values (i.e. grey value gradients >125) to the cost function, its contribution was weighted with a factor (α) (Equation 3.6). This factor is defined as the number of vertices corresponding to large gradient values divided by the total number of vertices.

$$CC(G_R, G_S) = \frac{\sum_{i=1}^M (\alpha G_R(i) - \bar{G}_{R,\alpha})(\alpha G_S(i) - \bar{G}_{S,\alpha})}{\sqrt{\sum_{i=1}^M (\alpha G_R(i) - \bar{G}_{R,\alpha})^2} \sqrt{\sum_{i=1}^M (\alpha G_S(i) - \bar{G}_{S,\alpha})^2}} \quad (3.6)$$

Finally, inconsistent gradient values between the bladder edge on the reference image and bladder edge on the CBCT image could result in segmentations with unrealistic large bladder volumes. These bladder volume explosions were prevented by adding a volume dependent value to the cost function (Equation 3.7). If the segmented volume (V_s) was above 125% of the full reference bladder volume (V_T) or below 75% of the empty reference bladder volume (V_T), the cost function value was increased with an additional volume dependent value.

$$CF^* = CF + \frac{|V_s - V_T|}{50} \quad (3.7)$$

Manual adaptations and model expansion

At the start of treatment, the patient-specific bladder shape model described the major bladder deformation pattern based on the full and empty bladder shape information. The use of this model assumed a bladder deformation during the course of treatment according to this deformation pattern. However, additional deformations during the course of treatment would not be taken into account. For example, the bladder could be locally deformed due to bowel filling during treatment which was not included in the model. As a consequence, the model was not able to segment the bladder correctly and manual local adaptations were needed to improve the bladder segmentation. This additional bladder shape information, obtained after manual adaptations, was used for optimizing the patient-specific bladder shape model during treatment.

If, after visual inspection of the result, the fully automatic segmentation strategy using the shape model proved insufficient, the observer could directly improve the segmentation by manually selecting correction points on the bladder edge. For each correction point the shortest distance to the segmented bladder surface mesh (P_{dist}) and its associated point of mesh intersection (P_{cp}) were determined (Figure 3.1). Next, mesh vertices of the bladder segmentation closest to P_{cp} (one if P_{cp} was a vertex point, two if P_{cp} was on an edge of a triangle or three if P_{cp} was on the face of a triangle) were shifted, parallel to the displacement vector from P_{cp} to the manually selected correction point, towards the manually selected correction point by the distance P_{dist} . Consequently, mesh vertices could be displaced in all three dimensions.

To prevent irregular bladder shapes or peaks in the bladder surface, vertices of connected triangular faces to P_{cp} vertices were also shifted using a scaled distance. If the distance P_{dist} was below 1.0 cm, the 1st, 2nd and 3rd order of connected vertices were shifted by scaling the distance P_{dist} by a factor 0.80, 0.50 and 0.20, respectively. If the distance P_{dist} was above 1.0 cm, the 1st, 2nd, 3rd and 4th order of connected vertices were shifted by scaling the distance P_{dist} by a factor 0.85, 0.60, 0.30, 0.10, respectively. After manual adaptation of the segmentation the entire bladder surface was smoothed using the previous described smoothing method to prevent unnatural shapes.

After segmentation using manual local adaptations, the resulting bladder shape described by spherical harmonic coefficients was added to the existing bladder shape model in order to optimize the patient-specific shape model. Consequently, new major modes of shape variation were calculated by determining new dominating eigenvectors. It was assumed that the sum of

all eigenvalues described 100% of the bladder shape variation. The dominating eigenvectors, determined by its eigenvalues describing 95% of the bladder shape variation, were used to build the expanded model. The new bladder deformation patterns were used to segment the bladder on the following CBCT images during treatment.



Figure 3.1 | Schematic overview of the manual local adaptation procedure (A) and an example of this procedure applied to improve the bladder segmentation, with the segmentation result obtained using the FA strategy in red (B) and the segmentation result obtained using the MAE strategy in yellow (C). From the manually defined correction point the closest point on the bladder surface mesh (P_{cp}) was determined and the associated distance (P_{dist}) was calculated. Mesh vertices closest to P_{cp} were shifted, parallel to the red dashed line, towards the manually selected correction point by the distance P_{dist} . Also, the 1st, 2nd and 3rd order vertices were shifted, indicated by the green (α), yellow (β) and orange (γ) arrow, respectively.

Segmentation validation

In this study, two segmentation strategies were performed and compared. The first strategy, the fully automatic (FA) strategy, consistently used only the shape model based on the full and empty bladder surfaces for segmentation without the use of manual adaptations. The second strategy, the manual adaptation and expanded (MAE) strategy, allowed manual local adaptations and the expanded shape model was used for the following segmentation.

To validate the segmentation results using the manual bladder delineations, all manual delineations were resampled in 3D using the previous defined sphere with 2091 evenly distributed vertices that was also used to resample the reference contours. After resampling, all manual delineations and segmentations consisted of an equal number of vertices and triangles.

We used the Dice similarity coefficient (DSC) to determine the volume overlap between the bladder segmentation and the manual bladder delineation. Given the manually delineated bladder structure ($Bladder_{Del}$) and the segmented bladder structure ($Bladder_{Seg}$), the DSC was defined as the volume of intersection divided by the average of both volumes (Equation 3.8).

$$DSC(Bladder_{Del}, Bladder_{Seg}) = 2 \frac{(Bladder_{Del} \cap Bladder_{Seg})}{(Bladder_{Del} + Bladder_{Seg})} \quad (3.8)$$

The contour-to-contour distances, i.e. the shortest distances between segmentation and manual delineation, were determined by calculating the shortest distance between each vertex of one mesh to an intersection with the other mesh. For each segmentation obtained using the FA strategy and the MAE strategy, the surface distance error (SDE) was defined as the mean of contour-to-contour distances.

The improvement of segmentation using manual adaptations and model expansion was studied by testing (Wilcoxon signed-rank test) the difference in segmentation results obtained using the FA strategy and the MAE strategy for the SDE, the DSC and the SD of contour-to-contour distances.

Besides the volume- and distance-based conformity test, the bladder volume determined by manual delineation was compared with the bladder volume determined by segmentation using the two strategies. For each patient group, a Bland-Altman error analysis was performed to determine the agreement between bladder volumes obtained by manual delineation and segmentation. The difference between obtained bladder volumes by manual delineation and segmentation was plotted against the average of obtained bladder volumes for both segmentation strategies and the 95% confidence interval of the error distribution was reported. In addition, the time needed to segment the bladder using the FA strategy and the MAE strategy was recorded.

To establish the efficacy of the expanded model on the segmentation results, an additional fully automatic with expanded model (FAE) segmentation strategy was performed. This FAE strategy was comparable to the FA strategy, but using the expanded shape model obtained during the MAE strategy instead of the shape model based on only the full and empty bladder surfaces. The improvement in segmentation results obtained using the FAE strategy compared to the FA strategy was tested (Wilcoxon signed-rank test) for both the DSC and SD of contour-to-contour distances.

3.3 | Results

For each patient, a unique patient-specific bladder shape model was built using surface meshes, described by 192 ($K=7$) spherical harmonic coefficients. One PCA mode was used to represent the bladder shape deformation in the model, which is associated with bladder volume change. After expanding the model with manually adapted surfaces, one to four PCA modes were used to represent bladder shape deformations. The second and third PCA mode modeled mainly translations and rotations of the bladder and higher order PCA modes modeled other deformation patterns.

In total, 119 CBCT images were used to validate the segmentation algorithm. Initialization of the segmentation procedure took 18 seconds on average and the computer needed 29 seconds on average to segment the bladder using the FA strategy. Bladder segmentation using the MAE strategy took 36 seconds on average and manual adaptation added 21 seconds on average to this

segmentation time. All segmentations were performed on a personal computer with a quad core, CPU of 3.20 GHz and 6.0 GB of RAM.

The DSC and the SD of the contour-to-contour distances between the segmentation and manual delineation, for the FA strategy as well as the MAE strategy, were plotted (Figure 3.2). The manual local adaptations yielded an increased agreement with the manually delineated volumes, as can be seen by the increased median DSC and decreased median SD of contour-to-contour distances. Although the mean SDE between the segmentation and manual delineation using the FA strategy was accurate, the use of the MAE strategy increased the agreement between the segmentation and manual delineation significantly ($p < 0.01$) for each group, indicated by a decreased mean SDE (Table 3.2). Moreover, the results obtained with the use of manual local adaptations (MAE strategy) were improved significantly for both the DSC ($p < 0.01$) (Figure 3.3a) and the SD of contour-to-contour distances ($p < 0.01$) (Figure 3.3b).

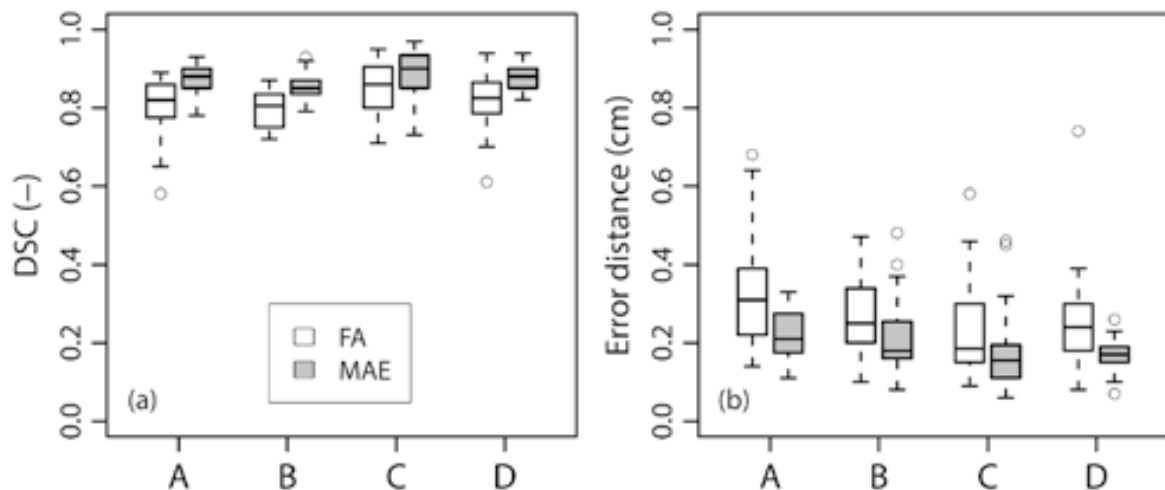


Figure 3.2 | Box-and-whisker plots of the DSC (a) and SD of contour-to-contour distances (i.e. error distance) (b) between manual delineations and segmentations, acquired according to the FA strategy and the MAE strategy, for each patient group defined on the x-axis. The box represents the upper and lower quartiles (IQR) and the band inside the box the median value. The whisker represents the largest (lowest) value still within 1.5 IQR of the upper (lower) quartile. Dots above or below the whiskers are considered as outliers.

The Bland-Altman error analysis between bladder volume obtained by manual delineation and bladder volume obtained using automatic segmentation is shown (Figure 3.4). The mean (SD) difference in bladder volume obtained by manual delineation and segmentation was 23 (90) ml and 11 (38) ml (female, prone), 15 (48) ml and -4 (23) ml (female, supine), 9 (27) ml and -1 (21) ml (male, supine) and 0 (35) ml and 1 (19) ml (male, prone) using the FA strategy and the MAE strategy respectively. The results showed that the 95% confidence interval of the error distribution decreased for all groups using the MAE strategy instead of using the FA strategy.

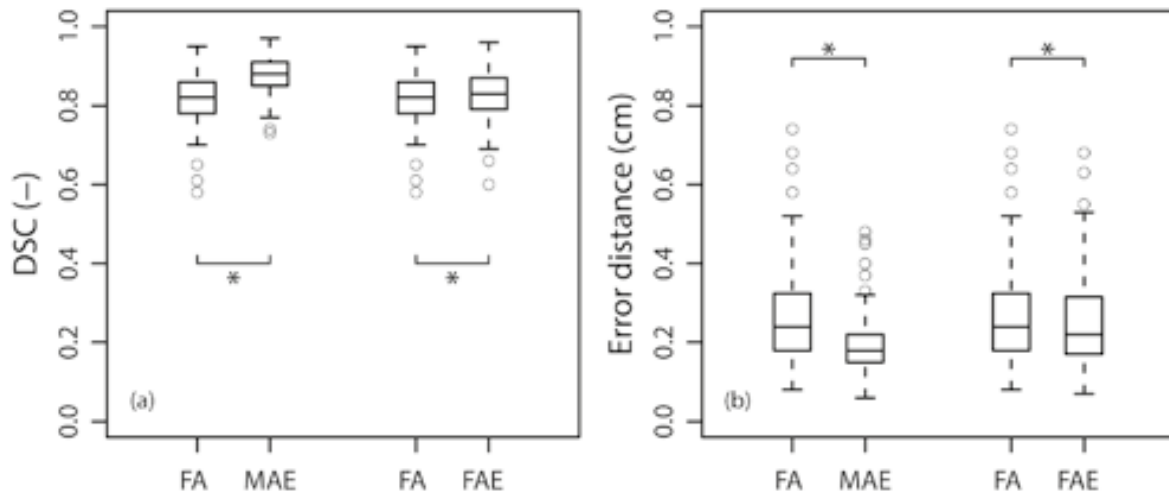


Figure 3.3 | Box-and-whisker plots of the DSC (a) and SD of contour-to-contour distances (i.e. error distance) (b) between manual delineations and segmentations for the FA strategy versus the MAE strategy and the FA strategy versus the FAE strategy. For the meaning of box, whiskers and dots: see Figure 3.2. Horizontal lines including an asterisks indicate statistical significant difference ($p < 0.01$).

Regarding the DSC (Figure 3.3a) and the SD of contour-to-contour distances (Figure 3.3b), the segmentations obtained using the FAE strategy instead of using the FA strategy were improved significantly ($p < 0.01$). Although an overall significant improvement was observed, the segmentation accuracy in 11% of the individual cases was improved substantially (i.e. increase of DSC > 0.05 or decrease of SD of contour-to-contour distances > 0.1 cm) to possibly be clinically beneficial (Figure 3.5). Using these criteria, the segmentation results obtained using the FAE strategy were worse compared to the segmentation results obtained using the FA strategy in only 2% of the cases.

Table 3.2 | Mean (range) surface distance error for each patient group using the FA segmentation strategy and the MAE segmentation strategy. Asterisks indicate a statistical significant difference ($p < 0.01$) between SDE obtained using the FA strategy and using the MAE strategy.

SDE (cm)	Group A *	Group B *	Group C *	Group D *
FA strategy	0.38 (0.15–0.76)	0.35 (0.12–0.70)	0.26 (0.10–0.58)	0.33 (0.10–0.78)
MAE strategy	0.27 (0.14–0.40)	0.28 (0.11–0.58)	0.21 (0.08–0.42)	0.23 (0.09–0.35)

Abbreviations: SDE = surface distance error; FA = fully automatic; MAE = manual adaptation and expanded.

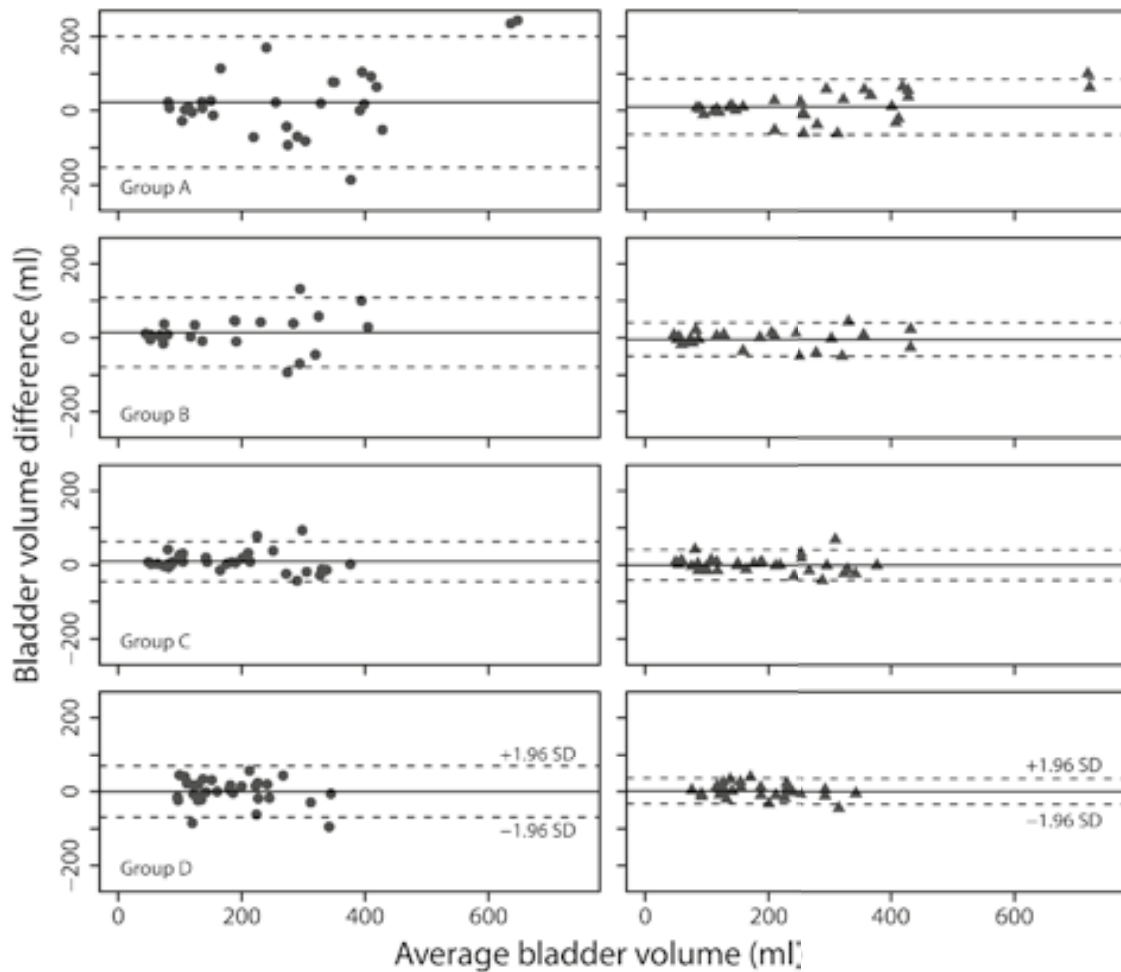


Figure 3.4 | Bland-Altman error analysis for bladder volumes obtained by manual delineation vs. bladder volumes obtained by segmentation using the FA strategy (dots; left column) and using the MAE strategy (triangles; right column) for each patient group separately. The horizontal solid line indicates the mean bladder volume difference and the horizontal dashed lines indicate the 95% confidence interval.

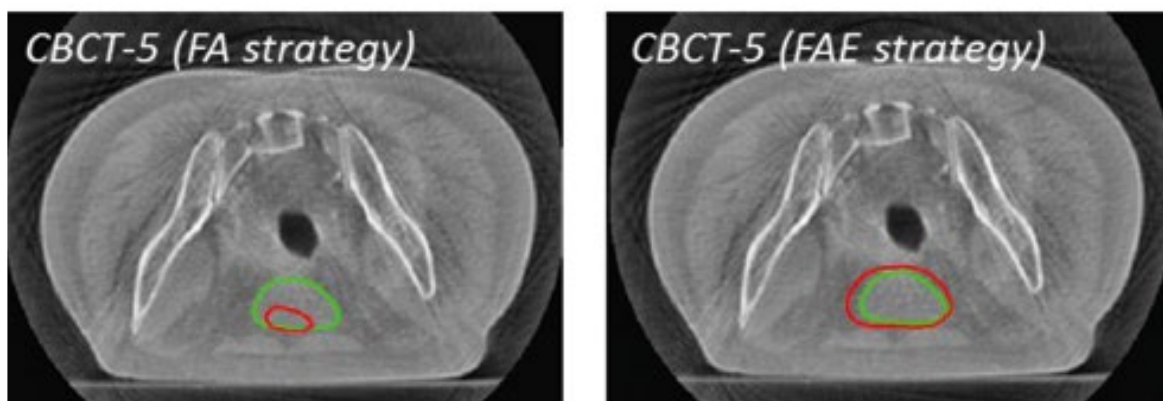


Figure 3.5 | An example of the difference in segmentation result for the fifth treatment fraction, obtained using the FA strategy (left) and using the FAE strategy (right) with the segmentation result (red) and manual delineation (green). Since this was the fifth CBCT to be analyzed for this patient, the model used in the FAE strategy also included shape information from manually adapted bladder segmentations of previous CBCT images of this patient.

3.4 | Discussion

We presented a method for automatic bladder segmentation on CBCT, independent of gender and the treatment position (prone or supine). Using a patient-specific bladder shape model based on a full and empty bladder structure, this method automatically produced an accurate bladder segmentation in a short time. Provided CT sets with a full and empty bladder are available, this segmentation strategy can be used from the first CBCT image during an adaptive radiation therapy treatment. This novel segmentation method contained several automatic correction strategies to avoid segmentation failure caused by the moderate CBCT image quality. In cases with less adequate results, the segmentation can be locally adapted by quick manual corrections. In addition, after manual adaptations the patient-specific bladder shape model can be expanded with the adapted segmentation to better optimize the patient-specific bladder shape model in subsequent CBCTs.

The bladder segmentation method presented in this study produced more accurate segmentations compared to previous reported results of bladder segmentation on CBCT by Chai *et al.* [106,107]: a higher mean DSC of 0.87 (0.79 and 0.78, respectively) and smaller SD of contour-to-contour distances of 0.19 cm (0.24 cm and 0.30 cm, respectively). Moreover, our mean DSC of bladder segmentation using the fully automatic strategy (0.82) was similar to the inter-observer bladder delineation variation on CBCT reported by Lütgendorf-Caucig *et al.* [112] (0.82) and Foroudi *et al.* [113] (0.75). Besides these accurate segmentations compared to previous reported studies on bladder segmentation on CBCT, this method is applicable from the start of ART with a plan-of-the-day approach without the need for a large training set. Furthermore, it was successfully applied and tested on male and female patients treated in both supine and prone position.

Since retrospective data were used in this study, the CBCT with the emptiest bladder was used as a surrogate to compensate for the absence of a second pre-treatment CT with empty bladder. Using this strategy, the patient-specific shape model included also possible rectum and bowel filling variability influencing the bladder shape. This additional information of shape deformation will not be included in the model when using two pre-treatment CTs. However, rectum and bowel filling variability influencing the bladder shape will also be present using two pre-treatment CTs for model building due to intrafraction motion of bowel and rectum [114]. Nevertheless, the bladder shape variation caused by rectum and bowel filling variability in the used strategy was probably increased due to the large time between scans used for shape modeling. Therefore, the results in this study contained a possible small bias in favor of our method due to the use of a CBCT scan as a surrogate.

Our patient population consisted of twenty patients, divided in four groups based on gender and the treatment position. A substantial number of patients was analyzed and the robustness of our method was verified by a large number of CBCTs. The data analyzed in this study were sufficient to show the efficacy of our proposed method for each patient group. However, for bladder cancer patients with the bladder being the target area instead of an OAR, the difference in flexibility between the bladder wall and tumor can influence the bladder deformation pattern [115].

Since the delineated bladder contours on CT images, used for model building, were all used clinically for treatment planning purposes, these CT-based bladder contours were of high quality. Due to the low inter-observer delineation variation of the bladder on CT [116], the input used for model building will not become more accurate when provided by different observers. Consequently, model input provided by different observers will have a very limited impact on segmentation results.

To acquire accurate bladder contours on CBCT images for validation purposes, delineations were performed by one observer and revised by a second observer. Although the inter-observer bladder delineation variation on CBCT is relatively low and revision by a second observer increased the delineation accuracy even more, the influence of inter-observer bladder delineation variability on our proposed automatic segmentation algorithm is of interest [112]. However, to fully determine this influence on our outcome would require a complete delineation study and was out of the scope of this study.

The manually delineated bladder contours on CBCT images were resampled using the uniform 3D sphere surface with its evenly distributed 2091 vertices for validation purposes. The determination of the central point (O_{sphere}) was performed automatically by calculating the center of the empty bladder contour. As observed by Chai *et al.* [106], the segmentation was not sensitive to this position if every point on the bladder surface was visible from O_{sphere} . Moreover, for a number of segmentations several positions of O_{sphere} were tested and minimal differences in segmentation results were observed. The number of evenly distributed vertices used to resample the manually delineated bladder contours on CBCT were assumed to be dense enough to fully describe the bladder surfaces. To verify this assumption, a 3D sphere with known radius was created and its volume was compared with the volume of this sphere obtained after our resampling strategy. Only 1% volume difference was observed between the volume of the sphere (114 ml) and the volume determined after resampling. Given this very small volume difference, the number of evenly distributed vertices is sufficient and the validation accuracy will not increase when using the original manually delineated bladder contours instead of the resampled manual delineations for validation purposes.

Incorrect bladder segmentations caused by image artefacts on CBCT were already observed by Chai *et al.* [107] and a failure rate (i.e. a very low similarity with the manually delineated bladder: $\text{DSC} < 0.65$) of 32% was reported. To avoid this relatively high failure rate caused by image artefacts on CBCT, automatic adaptations were implemented in our segmentation algorithm. The use of these automatic adaptations resulted in an overall failure rate of only 3%.

To locally improve bladder segmentations using manual adaptations, mesh vertices closest to the selected point and connected vertices were shifted towards this selected point, parallel to the displacement vector between P_{cp} and the manually selected correction point. The scaling factors used to shift connected vertices were tested and optimized on four randomly selected patients. Since these scaling factor values worked for our purpose, these values were not optimized and tested

on all patients. Moreover, after local manual adaptation the entire bladder surface was smoothed to prevent unnatural shapes which decreased the influence of these factors on segmentation outcome.

After each locally improved segmentation using manual adaptations, the patient-specific bladder shape model was expanded. The advantage of this strategy is the use of all available information of the patient instead of only the pre-treatment defined bladder shape information. Although the use of the expanded patient-specific shape model did improve the segmentation results significantly in terms of DSC (Figure 3.3a) and SD of contour-to-contour distances (Figure 3.3b), substantial improvement of the segmentation accuracy was observed only for some individual cases (Figure 3.5). This is probably caused by the use of only a relatively small number of CBCT images per patient. In the case of ART, daily CBCT images are acquired and the effect of model expansion will probably increase.

Our automatic procedure performed within the range of human observer variability, being the best standard presently available. This delineation variability should be accounted for in the planning margin around target volumes. In addition, automatic bladder segmentation can be applied to select the plan-of-the-day, as demonstrated for multiple-plan bladder ART by Chai *et al.* [107]. Whether our procedure also supports plan-of-the-day selection during multiple-plan ART for cervical cancer patients will have to be studied. For dose calculation and dose accumulation purposes, more accurate segmentations might be needed and therefore the CBCT image quality need to be improved or MRI can be considered for image guidance.

An alternative approach for automatic organ segmentation is the use of an atlas-based segmentation algorithm. A large number of successful studies reported on automatic segmentation on CT images using an atlas-based approach. Only one study reported about the application of such a method for bladder on CBCT [117]. They showed a mean DSC of 0.54, indicating a weak performance of atlas-based segmentation on CBCT. The main reason for failure using this atlas-based strategy is the relatively poor image quality of CBCT. However, our segmentation method is much better able to handle this relatively poor image quality.

The proposed automatic bladder segmentation method is especially applicable during multiple-plan bladder ART [60,99], because a library of bladder contours for designing multiple plans is already available and can also be used for bladder shape modeling. Moreover, the proposed segmentation method will be extremely suitable for online position verification purposes or online plan selection purposes during multiple-plan bladder ART. However, the total time of the segmentation process currently limits the online application and therefore the implementation of our segmentation method will be improved to speed up the process of segmentation.

Furthermore, our proposed automatic bladder segmentation method is also applicable during multiple-plan ART of the cervix-uterus for both supine and prone treatment position. Several studies reported on the correlation between bladder volume differences and the position of the cervix-uterus [64,83]. Given this correlation, daily size and position of the bladder determined by automatic segmentation can predict the position of the cervix-uterus and can be used for online

plan-of-the-day selection. In addition, the pre-treatment imaging acquired for cervix-uterus ART is also suitable to create a bladder shape model needed for segmentation on CBCT [83].

3.5 | Conclusion

The presented patient-specific bladder shape model, based on only pre-treatment imaging information, was suitable for automatic bladder segmentation on CBCT images. This method was independent of gender and treatment position and allowed for accurate automatic segmentation of the bladder on CBCT. Bladder segmentations can be improved locally using manual adaptations, which was easily incorporated into the workflow.